Binding of the *b*-Subunit in the ATP Synthase from *Escherichia coli*†

Manuel Diez,‡ Michael Börsch,*,§ Boris Zimmermann,‡ Paola Turina,|| Stanley D. Dunn,⊥ and Peter Gräber‡

Institut für Physikalische Chemie der Universität Freiburg, Albertstrasse 23a, D-79104 Freiburg, Germany, 3. Physikalisches Institut, Universität Stuttgart, Pfaffenwaldring 57, D-70569 Stuttgart, Germany, Dipartimento di Biologia Ev. Sper., Universitá degli Studi di Bologna, Via Irnerio 42, I-40126 Bologna, Italy, and Department of Biochemistry, University of Western Ontario, London, Ontario, Canada N6A 5C1

Received September 22, 2003; Revised Manuscript Received November 18, 2003

ABSTRACT: The rotary mechanism of ATP synthase requires a strong binding within stator subunits. In this work we studied the binding affinity of the *b*-subunit to F_1-ATPase of *Escherichia coli*. The dimerization of the truncated *b*-subunit without amino acids 1−33, b_{34-156}T62C, was investigated by analytical ultracentrifugation, resulting in a dissociation constant of 1.8 μM. The binding of *b*-subunit monomeric and dimeric forms to the isolated F_1 part was investigated by fluorescence correlation spectroscopy and steady-state fluorescence. The mutants b_{34-156}T62C and EF_1-γT106C were labeled with several fluorophores. Fluorescence correlation spectroscopy was used to measure translational diffusion times of the labeled *b*-subunit, labeled F_1, and a mixture of the labeled *b*-subunit with unlabeled F_1. Data analysis revealed a dissociation constant of 0.2 nM of the F_1b_2 complex, yielding a Gibbs free energy of binding of $\Delta G° = -55$ kJ mol^{-1}. In steady-state fluorescence resonance energy transfer (FRET) measurements it was found that binding of the *b*-subunit to EF_1-γT106C−Alexa488 resulted in a fluorescence decrease of one-third of the initial FRET donor fluorescence intensity. The decrease of fluorescence was measured as a function of *b*-concentration, and data were described by a model including equilibria for dimerization of the *b*-subunit and binding of *b* and b_2 to F_1. For a quantitative description of fluorescence decrease we used two different models: the binding of the first and the second *b*-subunit causes the same fluorescence decrease (model 1) or only the binding of the first *b*-subunit causes fluorescence decrease (model 2). Data evaluation revealed a dissociation constant for the F_1b_2 complex of 0.6 nM (model 1) or 14 nM (model 2), giving $\Delta G° = -52$ kJ mol^{-1} and $\Delta G° = -45$ kJ mol^{-1}, respectively. The maximal ΔG observed for ATP synthesis in cells is approximately $\Delta G = 55$ kJ mol^{-1}. Therefore, the binding energy of the *b*-subunit seems to be too low for models in which the free energy for ATP synthesis is accumulated in the elastic strain between rotor and stator subunits and then transduced to the catalytic site in one single step. Models in which energy transduction takes place in at least two steps are favored.

Proton transport coupled ATP synthesis in bacteria, chloroplasts, and mitochondria is catalyzed by membrane-bound H^+-ATP synthases. These enzymes have two large domains, a membrane-integrated F_0 part involved in proton transport and a hydrophilic F_1 part containing the nucleotide binding sites (for reviews see refs *1*−*4*). In *Escherichia coli*, the F_1 part has five different subunits with the stoichiometry $\alpha_3\beta_3\gamma\delta\epsilon$, and the F_0 part consists of three different subunits with a likely stoichiometry ab_2c_{9-14}. On the basis of functional studies, it was suggested that during catalytic turnover the catalytic nucleotide binding sites on the β-subunits adopt, in sequential order, three different conformations called "open", "tight", and "loose" according to their binding affinity to the nucleotides. These sequential changes of the binding affinity were generated by subsequent "docking−undocking" steps of the γ-subunit to the three $\alpha\beta$ pairs (*5*). The structure of the mitochondrial F_1 part has been solved to high resolution (*6*, *7*), and on the basis of a variety of structural and functional evidence, a model of the F_0F_1 complex was suggested. A rotating part ("rotor") formed by the γ- and ϵ-subunit of F_1 and the membrane-integrated *c*-ring moves during catalysis relative to a static part ("stator") which is formed by $\alpha_3\beta_3$, δ, b_2, and *a* (*8*). The rotation of the γ-subunit within $\alpha_3\beta_3$ has been visualized (for review see ref *9*) as well as the rotation of the *c*-subunit oligomer in the F_0 part (*9*, *10*). In EF_0F_1, stepwise γ-subunit rotation was monitored by a single-molecule FRET[1] approach during ATP hydrolysis (*11*) and, most recently, ATP synthesis (*12*, *13*).

The rotor−stator concept requires at least two connections between the F_0 and the F_1 part. Stimulated by this model, electron microscopic investigation of the H^+-ATP synthases from chloroplasts (*14*), from *E. coli* (*15*), and from mitochondria (*16*) revealed the existence of a second stalk. According to current views, this stalk is formed by two

† This work was supported by a grant from the Canadian Institutes of Health Research (to S.D.D.). The Biomolecular Interactions and Conformations Facility at the University of Western Ontario is supported by a Multi-user Maintenance and Equipment grant from the Canadian Institutes of Health Research. M.D. gratefully acknowledges financial support by the Graduiertenkolleg Ungepaarte Elektronen at the University of Freiburg.

* Corresponding author. Tel: +49 (0) 711-6854632. Fax: +49 (0) 711-6855281. E-mail: m.boersch@physik.uni-stuttgart.de.

‡ Universität Freiburg.

§ Universität Stuttgart.

|| Universitá degli Studi di Bologna.

⊥ University of Western Ontario.

10.1021/bi0357098 CCC: $27.50 © 2004 American Chemical Society
Published on Web 01/03/2004

b-subunits and attached to F_1 via the δ-subunit (*17*). A similar structure and a similar mechanism have been proposed for Na-translocating F-type ATPases (*18*).

With respect to the rotor−stator concept, since the torque exerted by the rotor subunits on the stator subunits needs to be resisted by the second stalk, it is important to know the strength of the binding between different elements of the stator. If the free energy for ATP synthesis is stored transiently as an elastic strain within the enzyme, the binding energy of the second stalk to the remaining F_0F_1 subunits must be at least as high as the energy for ATP synthesis. In living cells, the observed ΔG for ATP synthesis is about 55 kJ mol^{-1}, which would require a dissociation constant less than 0.2 nM between the second stalk and the remaining stator subunits (*19*).

The hydrophilic domain of the *E. coli b*-subunit was isolated and shown to form highly elongated dimers which bind to EF_1 with a K_d smaller than 1−2 μM (*20*). The interaction between the soluble *b*-dimer and the δ-subunit was found to be weak, $K_d = 5-10$ μM, calling for more extensive interactions of the *b*-dimer with $\alpha_3\beta_3$ (*21*). Such interactions were indicated both by cross-linking data (*22*, *23*) and by cryoelectron microscopy (*24*). Recently, the connection between the soluble b_2 and the F_1 stator subunits in a thermophilic bacterial enzyme has been shown to be strong (*25*).

The goal of the current work was to determine the strength of binding of the soluble *b*-subunit of *E. coli* to the F_1 part. After labeling genetically introduced cysteines in the γ-subunit of EF_1 and in the soluble *b*-subunit with different fluorophores, we carried out both fluorescence correlation spectroscopy (FCS) and steady-state FRET measurements and derived the binding constants of the complex between the soluble *b*, b_2, and F_1.

MATERIALS AND METHODS

Preparation and Labeling of Proteins. Strain pRA114/AN888, carrying the γT106C mutation, described in Aggeler and Capaldi (*26*), was a gift from the authors. EF_1 was isolated from the mutant strain as described (*27*) except that the ion-exchange chromatography was performed on a HQ 20 HPLC column (PerSeptive). The isolated EF_1 was stored in liquid nitrogen.

EF_1-γT106C was labeled in buffer A (50 mM MOPS/NaOH, pH 7.0, 100 mM NaCl, 2.5 mM $MgCl_2$) with different dyes essentially as described by Turina and Capaldi (*28*). The EF_1 concentrations were determined by UV absorption using the calculated extinction coefficient ϵ(280 nm) = 190730 M^{-1} cm^{-1} (*29*). All dyes were dissolved in dimethyl sulfoxide, and their concentrations were determined after a 1000-fold dilution with methanol using the following extinction coefficients given by the supplier (Molecular Probes): ϵ(541 nm) = 95000 M^{-1} cm^{-1} for tetramethylrhodamine-5-maleimide (TMR), ϵ(560 mn) = 92000 M^{-1} cm^{-1} for QSY-7-maleimide (QSY), ϵ(582 nm) = 108000 M^{-1} cm^{-1} for Texas Red-2-maleimide (TR), and ϵ(493 nm) = 72000 M^{-1} cm^{-1} for Alexa488-5-maleimide (Alexa488). EF_1-γT106C (20 μM) was incubated in buffer A, and the dye (dissolved in dimethyl sulfoxide in millimolar concentrations) was added to give a final concentration of 18 μM. After a reaction time of 4 min at room temperature unbound dye was removed by two subsequent passages through Sephadex G-50 centrifuge columns equilibrated with buffer A. The labeled enzymes were stored at −80 °C.

For investigation of the binding of the *b*-subunit to EF_1, we used a truncated *b*-subunit in order to facilitate the handling of the protein. In these truncated *b*-subunits, the hydrophobic part (amino acids 1−33) was removed, and a SYW leader sequence was added. Truncated *b*-subunits carrying a cysteine in position 62, b_{34-156}T62C, were prepared as described (*30*).

For labeling, 50 μM b_{34-156}T62C was incubated in buffer A in the presence of 100 μM TCEP with 100 μM dye (either TMR, TR, QSY, or Alexa488). After 15 min incubation at 30 °C excess reagent was removed by two consecutive passages through Sephadex G-50 centrifugation columns equilibrated with buffer A. The concentration of b_{34-156}T62C was determined by UV absorption spectroscopy in buffer A using the extinction coefficient ϵ(280 nm) = 7000 M^{-1} cm^{-1} (*29*). After labeling, the extinction coefficient at this wavelength increases strongly due to the absorbance of the fluorophores. Therefore, the protein concentration of the labeled b_{34-156}T62C was determined with the BCA protein assay (Pierce) using the unlabeled b_{34-156}T62C as a standard.

Analytical Ultracentrifugation. The dimerization constant K_1 of the soluble domain of *b* was determined by sedimentation equilibrium analysis in an analytical ultracentrifuge. A sample of purified b_{34-156} (*21*) was dialyzed into buffer containing 5 mM TES−NaOH, 100 mM NaCl, and 2.5 mM $MgCl_2$, pH 7.5. The protein concentration of the dialyzed sample was determined on the basis of absorbance in the far-UV (*31*). The protein was diluted to concentrations of 50, 100, and 200 μg/mL with the same buffer.

Sedimentation equilibrium experiments were performed using a Beckman Optima XL-A analytical ultracentrifuge in the Biomolecular Interactions and Conformations Facility at the University of Western Ontario. A four-hole An-60-Ti rotor and six channel cells with Epon charcoal centerpieces were used. Absorbance measurements were taken at 230 nm in 0.002 cm radial steps and averaged over ten observations. The cells were scanned immediately after starting the centrifuge to establish the relationship of absorbance to concentration. Samples were then allowed to equilibrate at 20 °C at rotor speeds of 20000, 25000, and 30000 rpm. Repeated scans were taken at 4 h intervals to ensure the equilibrium had been reached at each speed.

The data sets were processed, analyzed, and fitted to various models using Microcal Origin software and macros supplied by Beckman. Multiple data sets collected at different rotor speeds were fitted globally to determine the most appropriate model. The best fits were obtained for the monomer−dimer equilibrium model. The monomeric molecular mass calculated from the amino acid sequence was 13769. The partial specific volume was calculated as described by Zamyatin (*32*) to be 0.72 cm^3/g. The density

[1] Abbreviations: EF_1, hydrophilic F_1 part of the proton translocating H^+-ATPase from *Escherichia coli*; AMPPNP, β,γ-imidoadenosine 5′-triphosphate; MOPS, 3-morpholinopropanesulfonic acid; HEPES, 4-(2-hydroxyethyl)-1-piperazineethanesulfonic acid; TMR, tetramethylrhodamine-5-maleimide; Alexa488, Alexa488-5-maleimide; QSY, QSY-7-maleimide; TCEP, tris(2-carboxyethyl)phosphine hydrochloride; TES, *N*-[tris(hydroxymethyl)methyl]-2-aminoethanesulfonic acid; TR, Texas Red-2-maleimide; FCS, fluorescence correlation spectroscopy; FRET, fluorescence resonance energy transfer.

of the solvent was calculated by standard methods to be 1.002 g/cm^3. The dimerization constant K_1 was calculated from the fitted equilibrium constant and the starting protein concentrations and absorbances.

Fluorescence Correlation Spectroscopy (FCS). FCS was measured in buffer B after fluorescent impurities were removed by activated granular charcoal (1.5 mm, Merck). EF_1-γT106C−TMR and b_{34-156}T62C−TMR aliquots were diluted to final concentrations of 5×10^{-10} M. The fluorescence of single molecules was measured with an epi-illuminated confocal setup of local design (*11*). Fluorescence excitation was performed with a frequency-doubled Nd:YAG laser, 532 nm, cw (Coherent, Germany). The laser intensity was attenuated to 125 μW and focused by a water immersion objective (UPlanApo, 40×, NA 1.15; Olympus, Tokyo, Japan). Optics and mechanics were obtained from OWIS (Staufen, Germany) and modified. The dichroic mirror DCLP545 and interference filter HQ575/65 were obtained from AHF (Tübingen, Germany). The fluorescence signal was detected by a single photon counting avalanche photodiode (SPCM-AQR-15; EG&G, Vaudreuil, Canada). The multiplexed detector signal was registered in parallel by a multichannel scaler PC card (PMS 300; Becker & Hickl, Berlin, Germany) and by a real-time correlator PC card (ALV-5000/E; ALV, Langen, Germany) for FCS. The samples were measured on a microscope slide with a small depression covered with a conventional cover glass. The slide and cover glass were incubated with 100 μM unlabeled b_{34-156}T62C for 15 min. Excess b_{34-156}T62C was removed by washing the glass with buffer B. All measurements were performed at 20 °C. The actual detection volume (in the femtoliter range) was calculated from FCS data of rhodamine 6G in water.

For a quantitative interpretation of these data we used the following function (*33*):

$$g^{(2)}(t_c) = \frac{1}{N_F}\left\{\alpha\left(\frac{1}{1+t_c/t_{D1}}\right)\left(\frac{1}{1+(\omega_0/z_0)^2(t_c/t_{D1})}\right)^{1/2} + (1-\alpha)\left(\frac{1}{1+t_c/t_{D2}}\right)\left(\frac{1}{1+(\omega_0/z_0)^2(t_c/t_{D2})}\right)^{1/2}\right\} \times \{1 - T + T\exp(-t_c/t_T) - A + A\exp(-t_c/t_A)\} \quad (1)$$

In this equation N_F is the average number of fluorescent molecules in the confocal volume, $t_{D1} = \omega_0^2/4D_1$ is the characteristic time for translational diffusion of the molecules with the diffusion coefficient D_1, $t_{D2} = \omega_0^2/4D_2$ is the characteristic diffusion time for the molecules with diffusion coefficient D_2, A is the average fraction of molecules within a so-called dynamically quenched state, t_A is the characteristic correlation time of this quenched state, T is the average fraction of molecules in the excited triplet state with a characteristic triplet correlation time, t_T, α is the fraction of molecules with the smaller diffusion time t_{D1}, and ω_0 and z_0 are the radial and axial $1/e^2$ radii of the laser focus and detection volume.

Steady-State Fluorescence Measurements. Steady-state fluorescence measurements were performed in quartz cuvettes at 20 °C using a SLM Aminco 8100 spectrofluorometer. All spectra were recorded in the photon counting mode and corrected for lamp intensity. The labeled proteins were dissolved in buffer B (50 mM HEPES/NaOH, pH 8, 2.5 mM $MgCl_2$ and 100 mM NaCl). A quartz cuvette was filled with 270 μL of buffer B containing 50 nM labeled F_1, and the fluorescence intensity was recorded up to 1 h. To diminish exposure to excitation light, fluorescence was measured for a period of 1 min every 10 min until the fluorescence intensity reached a constant level. From the fluorescence decrease it can be concluded that approximately 30% of the initial F_1 concentration was adsorbed at the cuvette walls. In the FRET titration experiments the required amount of the labeled *b*-subunit was pipetted into the cuvette and gently mixed with a thin metal spatula. The spatula was preincubated in the same buffer with the same protein concentration as used in the cuvette.

For measurements of the binding kinetics, 30 μL of EF_1-γT106C−QSY was injected into 270 μL of b_{34-156}T62C−Alexa488 in buffer B with a Hamilton syringe. Mixing was completed within 1 s. Time traces of FRET donor intensity decrease were recorded with an integration time of 500 ms. The Förster radii for the FRET pairs Alexa488/TR and Alexa488/QSY are $R_0 = 6.0$ nm and $R_0 = 6.4$ nm, respectively, according to the supplier (Molecular Probes).

RESULTS

Dimerization Constant of b. Since the soluble domain of *b* has previously been shown to exist in a monomer/dimer equilibrium (*34*), it is essential to know the dimerization constant under the conditions where binding of *b* to F_1 was measured. Previously, dissociation constants for *b* constructs extending to the C-terminus have been reported only for 5 °C in the absence of Mg^{2+}, conditions under which the protein is well-behaved (*35*). Sedimentation velocity studies, however, have indicated that at 5 °C the C-terminal δ-binding domain is unfolded (*34*). At 20 °C, which permits the interaction of b_2 with δ (*21*), there is a slight tendency of b_2 to aggregate at higher concentrations, making determination of the dissociation constant more difficult.

To accurately determine the dimerization constant for the polar domain of *b* under conditions similar to those of the F_1-binding studies (2.5 mM $MgCl_2$, 20 °C), we carried out sedimentation equilibrium analysis of the b_{34-156} construct at low concentrations, determining the distribution of protein by the absorbance at 230 nm. A number of different rotor speeds were used to ensure the existence of a dynamic equilibrium between species present. As expected from earlier studies, attempts to fit the data to a single ideal species yielded average molecular masses intermediate between those expected for a monomer and dimer and poor fits of the data (not shown). In contrast, excellent fits were obtained using a monomer/dimer equilibrium model, as shown in Figure 1, yielding a dimerization constant of 1.8 μM under these conditions.

Fluorescent Labeling of Proteins. The γ-subunit of EF_1-γT106C was labeled with the maleimide derivatives TMR, Alexa488, or QSY as described in Materials and Methods. Figure 2 shows the SDS gel of EF_1-γT106C labeled with TMR under UV light excitation and after staining with Coomassie Blue, indicating an almost exclusive labeling of the γ-subunit. Only a weak fluorescence from the δ-subunit is observed, due to the short labeling time (4 min). The degree of labeling was 35−50% as determined from the UV/vis spectrum of the labeled EF_1 using the extinction coef-

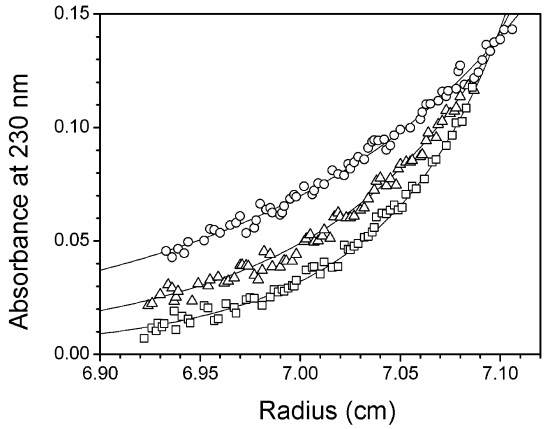

FIGURE 1: Sedimentation equilibrium analysis of the dimerization of b_{34-156}. Sedimentation equilibrium experiments were carried out at 20 °C as described in Materials and Methods. The starting protein concentration was 50 μg/mL. Data shown were collected after equilibration at rotor speeds of 20000 (circles), 25000 (triangles), and 30000 (squares) rpm. Three independent data sets from each rotor speed were globally fit to obtain the best value for the dissociation constant. The solid lines show the distribution of protein expected at each rotor speed for the fitted *b* value 1.8 μM.

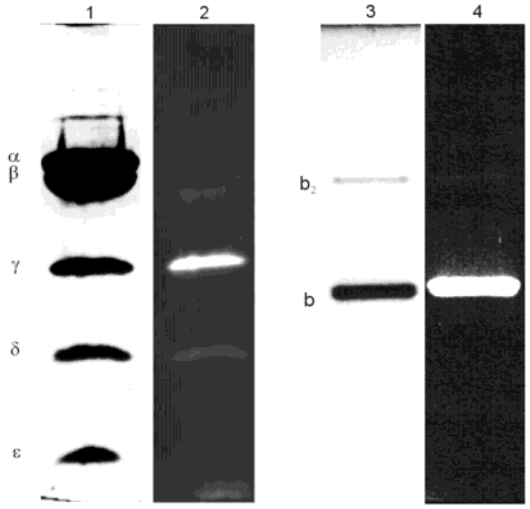

FIGURE 2: SDS gel electrophoresis of labeled of EF_1 and the *b*-subunit. Labeling of $EF_1\gamma$T106C with TMR and of the truncated b_{34-156}-subunit with Alexa488 was carried out as described in Materials and Methods. The free dye was removed by two passages through centrifugation columns, and 10 μg of protein per lane was used for the SDS−PAGE (15%). The unstained gel was documented under UV light and then stained with Coomassie Blue. Lanes 1 and 3 show $EF_1\gamma$T106C−TMR and b_{34-156}T62C−Alex488 after Coomassie Blue staining; lanes 2 and 4 show the same lanes under UV light.

ficients given in Materials and Methods. The absorption of the dye at 280 nm has been subtracted when the protein concentration was calculated. The specificity and the degree of labeling were similar for all three dyes used in this work. In addition, when wild-type EF_1 was treated with TR for a longer time (30 min), selective labeling of the δ-subunit was observed, with a degree of labeling of 60%.

For covalent labeling of the *b*-subunit with fluorophores, a cysteine was introduced at position 62, which is likely outside the dimerization interface of the *b* helix (*30*, *36*). Subunit b_{34-156}T62C was labeled with either TR, QSY, or Alexa488 so that it could be used either as a donor or as an acceptor in fluorescence resonance energy transfer (FRET)

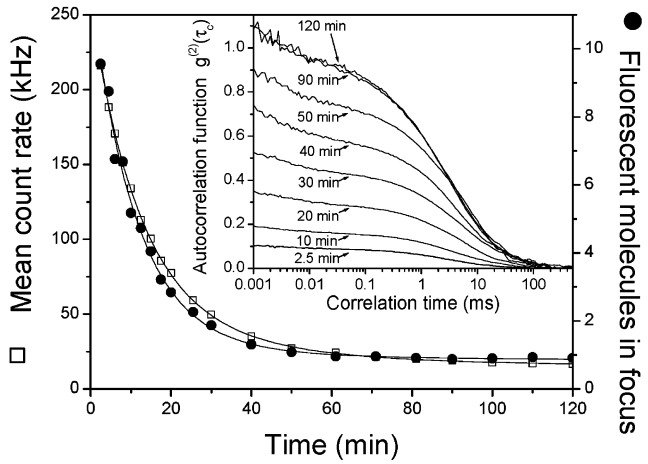

FIGURE 3: Adsorption of EF_1-γT106C−TMR. The FCS curves were measured with F_1-γT106C−TMR at different times (2.5−120 min) after placing buffer B with $[EF_1\text{-}\gamma T106C\text{−}TMR]_0 = 5$ nM on the microscope slide (inset). The data collection time for one curve was 30 s. The number of fluorescent molecules in the confocal detection volume was calculated from the autocorrelation functions and plotted as a function at time after the sample was pipetted on the slide. The decrease reflects adsorption of the labeled protein at the glass walls.

experiments, or it was labeled with TMR for FCS experiments. In addition to the band at the molecular mass of the truncated *b*-subunit, the SDS gel stained with Coomassie Blue (Figure 2) shows a faint band running at the molecular mass of the *b*-dimer. This band is not revealed by UV illumination, implying that this small fraction of the *b*-subunit is partly dimerized via a disulfide at Cys 62. The degree of labeling was determined as described in Materials and Methods. It resulted in approximately 40% for Alexa488, 20% for QSY, 73% for TR, and 65% for TMR.

Fluorescence Correlation Spectroscopy. In earlier work we used FCS to measure the diffusion coefficient of labeled EF_1, and we were able to detect conformational changes of EF_1 induced by substrate binding (*37*). Here we use this technique to estimate the binding strength of the *b*-subunit to EF_1. In the first FCS experiments we noticed a strong time dependency of the number of fluorescing molecules when the same concentration of labeled protein was used. One possibility for this effect is that at low concentrations the adsorption of the protein to the glass surface of the microscope slide plays a significant role.

To clarify this effect, we monitored the fluorescence autocorrelation functions at different times after addition of 85 μL of EF_1-γT106C−TMR (5 nM) in buffer B on a microscope slide. Figure 3, inset, shows the recorded autocorrelation functions. Its reciprocal amplitude is proportional to the number of fluorescing molecules in the confocal detection volume (see eq 1), and this number is plotted in Figure 3 as a function of time. There is a strong decrease of the average number of molecules (half-life time approximately 10 min) reaching a constant value after about 90 min. Since the initial concentration of EF_1-γT106C−TMR was 5 nM, the final concentration after 90 min corresponds to 0.5 nM, the difference being adsorbed at the glass surface. A similar effect has been reported in FCS studies of the isolated δ-subunit (*19*).

To determine the binding of the *b*-subunit to EF_1, we measured the following samples: (1) b_{34-156}T62C−TMR,

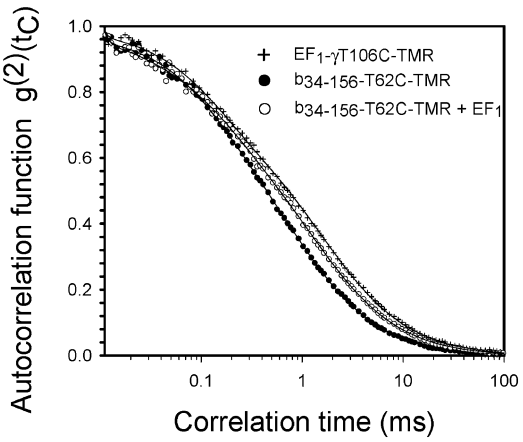

FIGURE 4: Fluorescence correlation spectroscopy of EF_1-γT106C−TMR and b_{34-156}T62C−TMR. Fluorescence autocorrelation functions were measured with b_{34-156}T62C−TMR (closed circles), with EF_1-γT106C−TMR (crosses), and with b_{34-156}T62C−TMR in the presence of unlabeled EF_1 (open circles) within 3 min after addition to the slide. The concentrations of b_{34-156}-T62C−TMR, of EF_1-γT106C−TMR, and of unlabeled EF_1 were 0.5, 5, and 22 nM, respectively. All proteins were dissolved in buffer B. The data were fitted with the autocorrelation function (eq 1) (solid lines) as described in Materials and Methods. The fit parameters are collected in Table 1.

(2) EF_1 labeled with TMR, and (3) b_{34-156}T62C−TMR in the presence of unlabeled EF_1. The fluorescence data were collected within a time interval of 30 s, 3 min after addition of the sample to the slide. We assume that under these conditions the initial concentrations were not changed significantly. The normalized autocorrelation functions are collected in Figure 4. Distinct differences between the three experiments, due to the different correlation times for translational diffusion, are apparent. b_{34-156}T62C exhibits the shortest diffusion time, EF_1 the longest diffusion time, and the mixture of EF_1 and b_{34-156}T62C an intermediate value. Since the autocorrelation data are normalized, these differences do not depend on the concentration of the fluorophore; when they were measured at different times after addition of the labeled protein to the microscope slide, the same result was always obtained.

For a quantitative interpretation eq 1 was used. This equation contains two diffusion terms, since we expect two species (b_{34-156}T62C−TMR and the complex b_{34-156}T62C−TMR/EF_1) with different diffusion times. The equation has an additional "bunching term", *A*, that represents a dynamically quenched state. This term is only necessary for a description of the protein-bound fluorophore TMR as it reflects a property of the fluorophore in the protein environment (*37*), whereas it was not used to fit FCS data of freely diffusing rhodamine 6G.

The normalized fluorescence autocorrelation data in Figure 4 were fitted with eq 1. For b_{34-156}T62C−TMR and for EF_1-γT106C−TMR we used eq 1 with $\alpha = 1$. Results of these fits are shown as solid lines in Figure 4, and the fit parameters are collected in Table 1. The autocorrelation function of b_{34-156}T62C−TMR in the presence of 22 nM unlabeled EF_1 was fitted with eq 1 using the fit parameters from the autocorrelation function of the labeled *b*-subunit (Table 1). For the diffusion time t_{D2}, the value obtained from the EF_1-γT106C−TMR diffusion measurements was used (Table 1); i.e., we assumed that the characteristic diffusion times of

Table 1: Results of the Fluorescence Correlation Spectroscopy Data Analysis

compound	t_{D1} (ms)	t_T (μs)	T	A	t_A (ms)	t_{D2} (ms)	α
*b*T62C−TMR	0.78	2.5	0.24	0.16	0.12	0	1
EF_1-γT106C−TMR	1.59	2.5	0.27	0.19	0.13	0	1
*b*T62C−TMR + EF_1	0.78[a]	2.5[a]	0.24[a]	0.16[a]	0.12[a]	1.59[b]	0.48

[a] Data from *b*T62C−TMR diffusion. [b] Data from EF_1-γT106C−TMR diffusion.

EF_1-γT106C−TMR and EF_1-*b*T62C−TMR are identical. With these assumptions, only the fraction α and the total number of fluorescent molecules in the confocal volume N_F are free parameters in the fit.

Analysis of Fluorescence Correlation Spectroscopy Data. From these data we calculated the K_d for binding of b_2-subunits to F_1 using the following general reaction scheme, which allows for the potential binding of both the monomeric and dimeric forms of subunit *b* to F_1.

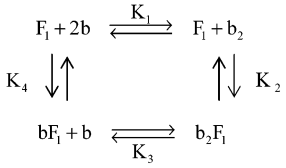

$$K_1 = [b]^2/[b_2] \quad (2)$$

$$K_2 = [b_2][F_1]/[b_2F_1] \quad (3)$$

$$K_4 = [b][F_1]/[bF_1] \quad (4)$$

$$K_3 = [b][bF_1]/[b_2F_1] \quad (5)$$

With these definitions we obtain

$$K_1K_2 = K_3K_4 = K_p = [b]^2[F_1]/[b_2F_1] \quad (6)$$

FCS data do not allow us to distinguish different fluorescent species. We can only distinguish between two groups of molecules, one with a short diffusion time, i.e., *b* and b_2, and one with a long diffusion time, i.e., bF_1 and b_2F_1. The total concentration of fluorescent molecules N_T is given by

$$[N_T] = [b] + [b_2] + [bF_1] + [b_2F_1] \quad (7)$$

The fraction α of fast diffusing molecules is

$$\alpha = \frac{[b] + [b_2]}{[N_T]} \quad (8)$$

Correspondingly, the fraction of slowly diffusing molecules is

$$1 - \alpha = \frac{[bF_1] + [b_2F_1]}{[N_T]} \quad (9)$$

Using eqs 2−9 the equilibrium concentrations of all species can be expressed as functions of the initial concentrations, $[b]_0$ and $[F_1]_0$, α, $[N_T]$, K_1, and the ratio K_4/K_3 (see Appendix A).

The initial concentrations in the experiment shown in Figure 4 were $[b]_0 = 0.5$ nM and $[F_1]_0 = 22$ nM. From analysis of the FCS data we obtained $\alpha = 0.48$ (see Table 1), and K_1 is known from the sedimentation equilibrium analysis to be 1.8 μM. The only unknown parameters are $[N_T]$ and K_4/K_3. By choosing $K_4/K_3 = 1$ (no cooperativity) and $K_4/K_3 = 10$ (positive cooperativity), $[N_T] = 0.496$ and $[N_T] = 0.340$ are obtained from eq A8. With $K_4/K_3 = 0.1$ (negative cooperativity) there was no solution. Equilibrium concentrations of all species were calculated with $[N_T] = 0.496$ and $[N_T] = 0.340$, from which $K_2 = 0.2$ and 0.002 nM, respectively, were obtained. These data indicate significant binding of the b_{34-156}T62C−TMR dimer to EF_1 at nanomolar concentrations.

Steady-State Fluorescence Measurements. During measurements of fluorescence spectra of labeled EF_1, we noticed that its fluorescence was partially quenched upon addition of the *b*-subunit. In our first series of measurements we observed a large scattering of the data, especially at low *b* concentrations. One effect that must be taken into account is the adsorption of protein at the surface of quartz cuvettes and the fact that relative fluorescence change due to this adsorption increases with decreasing concentration of the fluorescence labeled protein. To obtain reproducible results, the procedure given in Materials and Methods had to be followed very strictly.

In Figure 5 the fluorescence spectra of EF_1-γT106C−Alexa488 in the presence of increasing concentrations of b_{34-156}T62C−TR are shown. The fluorescence intensity at 518 nm decreased with increasing *b* concentration. The decrease saturated at high *b* concentrations, indicating that it was due to *b*-subunit binding to F_1. Extrapolation to high *b* concentrations indicated a maximal fluorescence decrease of $^1/_3$. In addition, a fluorescence increase at 610 nm was observed due to the emission of b_{34-156}T62C−TR (data not shown). The increase of fluorescence at 610 nm indicated a certain efficiency of FRET between the EF_1-γT106C−Alexa488 and the b_{34-156}T62C−TR as expected from a Förster radius of approximately $R_0 = 6.0$ nm. Further analysis of these data revealed that the fluorescence increase at 610 nm was only partly due to energy transfer and mainly reflected a direct excitation of b_{34-156}T62C−TR at the wavelength used for Alexa488 excitation.

Surprisingly, a fluorescence decrease was also observed upon addition of unlabeled b_{34-156} and of the longer *b*-subunit, b_{24-156}. Extrapolation to high *b* concentrations revealed in both cases a maximal fluorescence quenching of about $^1/_6$ of the initial fluorescence (data not shown). The reason for fluorescence quenching by the unlabeled *b*-subunit is not clear. One possibility is a direct interaction of a tryptophan in subunit *b* with Alexa488 bound at the γ-subunit. Subunit b_{34-156} contains a tryptophan in the leader sequence SYW, which was introduced to allow spectrophotometric measurement of the protein concentration, and similarly, the native *b*-subunit contains a tryptophan at position 26. We investigated fluorescence quenching of the fluorophore Alexa488 by tryptophan in buffer A and measured fluorescence intensities and fluorescence lifetimes as a function of tryptophan concentration. The data could be described by the Stern−Volmer equation, and their evaluation showed that Alexa488 fluorescence is dynamically quenched by tryptophan with a quenching constant $K = k_q\tau_0 = 7.7\ M^{-1}$ (lifetime of Alexa488 fluorescence $\tau_0 = 3.9$ ns; rate constant $k_q = 3.8 \times 10^9\ M^{-1}\ s^{-1}$). In this work we have taken advantage of the combined FRET and quenching effect, resulting in the fluorescence decrease at 518 nm, as a measure of *b*-subunit binding to F_1.

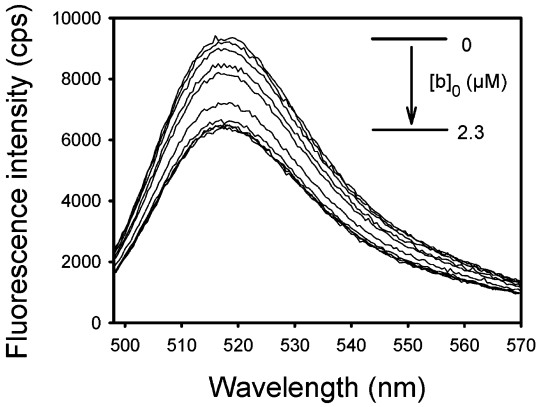

FIGURE 5: Fluorescence spectra of EF_1-γT106C−Alexa488 at different concentrations of the *b*-subunit. EF_1-γT106C was labeled with Alexa488, and its fluorescence spectrum was recorded (concentration 33 nM in buffer B, excitation at 488 nm). Different concentrations of b_{34-156}T62C−TR in buffer B (up to 2.3 μM) were added.

Kinetics of b-Subunit Binding to F_1. The kinetics of *b*-subunit binding to EF_1 could be followed by the kinetics of fluorescence decrease. Figure 6 (upper panel) shows the fluorescence of b_{34-156}T62C−Alexa488 and the effect upon addition of EF_1-γT106C−QSY. After a rapid decrease due to dilution, the fluorescence intensity decreased more slowly, indicating the binding of the labeled b_{34-156}T62C−TR to F_1−QSY. The inset shows as a control the addition of the same volume of buffer, where only the dilution effect is observed. The fluorescence decrease due to binding was measured for different EF_1 and *b* concentrations. These data are shown in Figure 6 (lower panel). Under these conditions, half-maximal decrease was obtained after about 5 s.

Analysis of Steady-State Fluorescence Data. The relative fluorescence decrease $\Delta F/\Delta F_{max}$ multiplied by $[F_1]_0$ was calculated from the data in Figure 5 and plotted as a function of initial *b* concentration (Figure 7). The data were initially fitted with an arbitrary sigmoidal function. The best fit value for the *b* concentration resulting in half-maximal fluorescence decrease, $[b(^1/_2)]_0$, was 67 nM. For a quantitative evaluation of the data, we used two different models: In model 1 the binding of the first *b*-subunit leads to the same fluorescence decrease as the binding of the second *b*-subunit, and binding of both monomers results in the same fluorescence decrease as that of b_2 binding. In model 2 the binding of the first *b*-subunit leads to the maximal fluorescence decrease; i.e., binding of the second *b*-subunit does not contribute to fluorescence decrease.

The relations between fluorescence decrease $[F_1]_0\ \Delta F/\Delta F_{max}$ and the initial *b* concentration are derived in Appendix B (eqs A15 and A16 for model 1 and eqs A20 and A21 for model 2). Figure 7 (upper panel) shows the curves calculated according to model 1 for different K_4/K_3 ratios. The solid line has been obtained for $K_4/K_3 = 1$, the dashed curve for $K_4/K_3 = 10$, the dotted curve for $K_4/K_3 = 0.1$, and the dot−dashed curve for $K_4/K_3 = 0.01$. In Figure 7 (lower panel) curves were calculated according to model 2 for the same

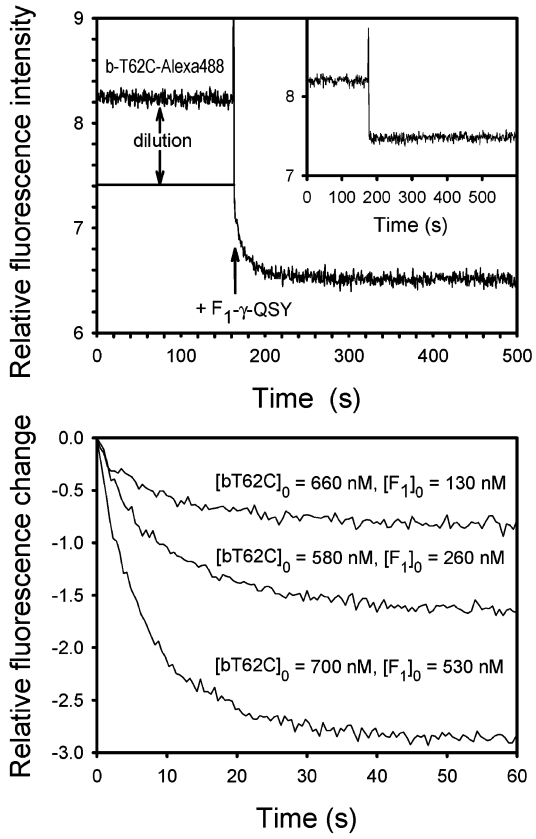

FIGURE 6: Kinetics of *b*-subunit binding to EF_1. Top: The fluorescence intensity of labeled b_{34-156}T62C−Alexa488 (660 nM in buffer B) was measured at 518 nm. At $t = 150$ s, EF_1-γT106C−QSY was added. The immediate decrease of the fluorescence is due to the dilution, as shown in the inset where the same volume of buffer B is added instead of F_1. The slow decrease of fluorescence indicates the binding of b_{34-156}T62C−Alexa488 to EF_1-γT106C−QSY. Bottom: Kinetics of the fluorescence changes at different EF_1-γT106C−QSY concentrations.

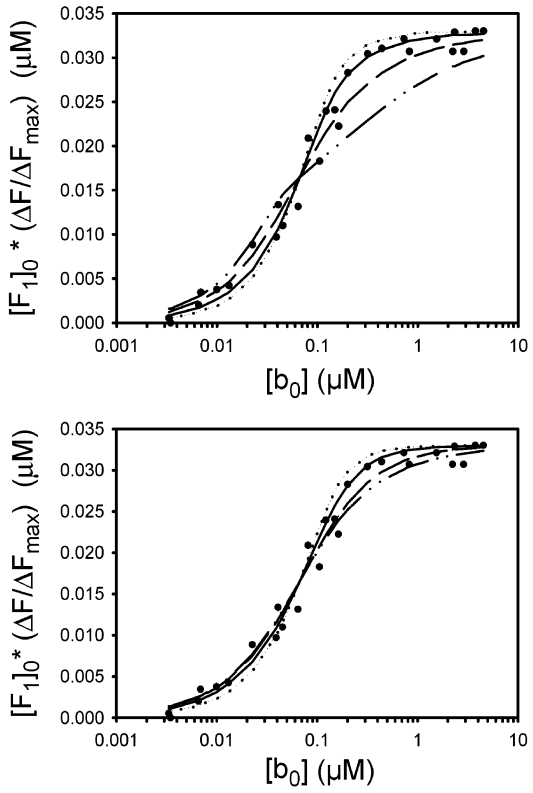

FIGURE 7: Relative fluorescence change of EF_1-γT106C−Alexa488 at 518 nm as a function of the concentration of b_{34-156}-T62C−TR. The relative fluorescence decrease of labeled EF_1 (initial concentration 33 nM) was measured at 518 nm as a function of the initial concentration of b_{34-156}T62C−TR. Data are from Figure 5 and additional measurements. Both proteins were dissolved in buffer B. The concentration of *b* changes from 3 nM to 2.3 μM. Curves were calculated according to model 1 (eqs A15 and A17) (top) and model 2 (eqs A20−A23) (bottom), respectively, with the parameter $K_4/K_3 = 1$ (solid line), $K_4/K_3 = 0.1$ (dashed line), $K_4/K_3 = 10$ (dotted line), and $K_4/K_3 = 0.01$ (dot−dashed line).

K_4/K_3 ratios. These data are collected in Table 2 with the corresponding standard deviations from the experimental data. The smallest standard deviation is observed at the ratio $K_4/K_3 = 1$ for model 1 and $K_4/K_3 = 0.1$ for model 2, i.e.

$$K_1 = 1.8\ \mu\text{M},\ K_2 = 0.6\ \text{nM},\ K_3 = 33\ \text{nM},\ K_4 = 33\ \text{nM} \quad \text{(model 1)}$$

and

$$K_1 = 1.8\ \mu\text{M},\ K_2 = 14\ \text{nM},\ K_3 = 509\ \text{nM},\ K_4 = 51\ \text{nM} \quad \text{(model 2)}$$

For comparison we specifically labeled the δ-subunit of the wild-type EF_1 with TR and titrated $F_1\delta$−TR with b_{34-156}-T62C−Alexa488. Again a fluorescence decrease was observed, but significantly higher concentrations of b_{34-156}-T62C−Alexa488 ($[b(^1/_2)]_0$ was about 500 nM) were necessary to obtain the maximal fluorescence decrease. We conclude that labeling of the δ-subunit impairs the binding of b_{34-156} so that the dissociation constant is significantly increased compared to the dissociation from nonlabeled EF_1. Presumably, the labeled cysteine in the δ-subunit is located at the interface between the δ- and the *b*-subunit. If this is true, labeling of this cysteine should not occur in the wild-type holoenzyme EF_0F_1. Indeed, no labeling of the δ-subunit in EF_0F_1 was observed under the same conditions as for labeling the δ-subunit in EF_1, consistent with the proposed interpretation. It is known that fluorescence labeling of the δ-subunit occurs at Cys 140, which is located near the C-terminus (*38*, *39*). This region has been shown to be near the binding site for the *b*-subunit (*40*).

Table 2: Equilibrium Constants of the Binding of Subunit *b* to EF_1[a]

	K_4/K_3	K_2/nM	K_3/nM	K_4/nM	σ
model 1	0.01	0.60	328	3.28	3.62×10^{-3}
	0.1	0.60	104	10.4	1.82×10^{-3}
	1	0.60	33	33	1.78×10^{-3}
	10	0.60	10.4	104	2.27×10^{-3}
model 2	0.01	130	4828	48	1.72×10^{-3}
	0.1	14	509	51	1.55×10^{-3}
	1	2.6	68	68	1.70×10^{-3}
	10	1.04	13.7	137	2.24×10^{-3}

[a] The fluorescence decrease of EF_1-γT106C−Alexa488 was measured and analyzed according to either model 1 or model 2 as described in the text. The equilibrium constant for dissociation of b_2 was $K_1 = 1.8$ μM. Curves were calculated for different ratios of K_4/K_3, and K_2 was calculated from the fit or from eqs A18 and A22. σ is the root mean square deviation calculated between the set of experimental points and the calculated values.

DISCUSSION

The interaction energy among the stator subunits of F_0F_1 is of special importance for the mechanism of ATP synthesis.

It has been proposed that the free energy derived from proton translocation through the enzyme is transiently stored in conformational energy of the protein (*5*). In particular, since it was shown that the γ-subunit rotates with respect to the $\alpha_3\beta_3$ complex during ATP hydrolysis (*41*−*43*), it is generally assumed that this energy is transiently stored in the elastic deformation of the γ-subunit. Different models have been discussed. Some authors have favored a mechanism in which the energy of the three to four protons required for synthesis of one ATP molecule is stored as a whole in the γ-subunit until it is transduced to the catalytic site for ATP synthesis (*19*, *44*). This mechanism requires that the interaction of stator subunits must be at least as strong to withstand the highest energy necessary to release ATP, or intrinsic uncoupling will occur. Since the highest ΔG observed in ATP synthesizing organelles is approximately 50−55 kJ mol^{-1}, the interaction energy between the second stalk and the remaining stator subunits should be higher than 50−55 kJ mol^{-1}. Alternatively, other authors suggest that the energy of the proton gradient is transduced to the catalytic site in a gradual manner (*45*, *46*), in which case the elastic torque stored in the γ-subunit would not need to be higher than that involved in each single step. According to Oster and Wang (*45*), the gradual energy transduction is essential for explaining the high transduction efficiency calculated for the ATP synthase.

The second, or peripheral, stalk of EF_0F_1, constituted by the δ- and b_2-subunits, has two interfaces to the remaining subunits of EF_0F_1, one within the membrane (with the ac_{9-14} subcomplex) and one outside the membrane (with the $\alpha_3\beta_3$ subcomplex). Both of them need to resist the elastic strain transiently stored in the γ-subunit. In this work we have investigated the interaction outside the membrane. The δ subunit binds to the N-terminal regions of the α-subunits near the top of the enzyme (*24*). The polar region of b_2 binds to δ (*21*, *22*) but also interacts directly with $\alpha_3\beta_3$ (*23*). These latter interactions may provide an important part of the overall binding energy of b_2. The most critical binding parameters regarding the second stalk are therefore those describing the interaction of b_2 with F_1-ATPase, which includes the δ-subunit. We were able to address this interaction specifically, avoiding contributions of other parts of F_0 with F_1, by using the soluble form of *b* lacking the membrane-binding domain. The soluble b_2 protein is capable of competing with F_0 for binding to F_1 (*20*), implying that it binds to F_1 in the normal way; chemical cross-linking analysis also supports this idea (*23*). In the soluble form lacking the membrane-spanning domains, however, *b* exists in a monomer−dimer equilibrium (*34*). By careful measurement of the dimerization constant under conditions similar to those used for studying the interaction of *b* with F_1, this equilibrium has been incorporated into our calculations of the dissociation constant of the b_2−F_1 complex.

The binding of the soluble portion of the *b*-subunit to isolated EF_1 has been monitored by FCS and steady-state FRET. Fluorescence correlation spectroscopy was used to determine the diffusion times of EF_1-γT106C−TMR and b_{34-156}T62C−TMR. In a mixture of 0.5 nM b_{34-156}T62C−TMR and 22 nM unlabeled EF_1, species with two different diffusion times were found. We interpreted the free b_{34-156}-T62C−TMR and its dimer as the species with the short diffusion time and the labeled bF_1 and b_2F_1 complexes as the species with the longer diffusion time. Under these experimental conditions, approximately half of b_{34-156}T62C−TMR was bound to EF_1, which allowed us to evaluate a dissociation constant K_2 of 0.2 nM.

The binding of the labeled b_{34-156}T62C−TR to EF_1-γT106C−Alexa488 leads to a decrease of the FRET donor fluorescence intensity at 518 nm, and this has been used to determine the dissociation constant. Extrapolation to high *b* concentrations indicated a decrease of one-third of the fluorescence. However, when the unlabeled b_{34-156}T62C was used for binding, extrapolation to high *b* concentrations indicated that maximally one-sixth of the fluorescence of the γ-labeled EF_1 can be quenched in the absence of a FRET acceptor. The reason for this effect might be a dynamic quenching of the fluorophore at the γ-subunit by the Trp in the *b*-subunit. Alternatively, the fluorescence quenching upon *b*-subunit binding could also be caused by conformational changes transmitted to the γ-subunit from the $b_2/\alpha_3\beta_3$ interface resulting in a decrease of fluorescence quantum yield.

The fluorescence decrease of EF_1-γT106C−Alexa488 with increasing concentrations of b_{34-156}T62C−TR has been analyzed assuming binding equilibria between all species. The curves shown in Figure 7 (top) have been obtained with the assumption that the species bF_1 shows half of the decrease relative to the b_2F_1 species (model 1, eq A14). The value of 1.8 μM for K_1, determined by analytical ultracentrifugation, has been used in all calculations, leaving as the only unknown parameters K_2 and the ratio K_4/K_3 (the value of the fourth equilibrium constant results from the necessary condition that $K_1K_2 = K_3K_4$). On the basis of the *b* concentration required for half-maximal decrease (see Figure 7), it resulted $K_2 = 0.6$ nM with $K_4/K_3 = 1$. This K_4/K_3 ratio generated the curve with the smallest standard deviation from the experimental data. Under the alternative assumption that binding of the first *b*-subunit leads to full fluorescence decrease (model 2), eq A19 was obtained. The lines in Figure 7 (bottom) have been calculated using this assumption and $K_1 = 1.8$ μM. The standard deviation in this case showed a minimum for the ratio $K_4/K_3 = 0.1$, resulting in $K_2 = 14$ nM. These data favor a model with no, or a negative, cooperativity for binding of the second *b*-subunit.

In conclusion, according to our data, the dissociation constant for the truncated, dimeric b_{34-156} subunit binding to EF_1, K_2, is between 0.2 and 14 nM. With $\Delta G° = -RT \ln K_2$ we obtain Gibbs free energies of binding between −55 and −45 kJ mol^{-1}. These values are similar or below the Gibbs free energy of ATP synthesis in vivo. While it is possible that the anchoring of the normal b_2 in the membrane may affect the affinity for F_1 in a way that has not been accounted for in this analysis with soluble *b*, the similarity of the interactions of the two forms of *b* with F_1 implies that any such effect will be small. Indeed, after cross-linking the γ-subunit to the soluble portion of b_2 in the thermophilic bacterium PS3, the $b_2/\alpha_3\beta_3\delta$ interface was shown to withstand the torque induced in the γ-subunit by ATP hydrolysis (*25*).

For a coupled mechanism of elastic strain transduction it is expected that the binding energy of the b_2-subunit is significantly higher than each step in the mechanochemical mechanism leading to ATP synthesis. Our data show that the binding energy of b_2 to F_1 is of similar magnitude or

smaller than the free energy of ATP synthesis. In current models of rotational catalysis, energy is transduced stepwise from rotation of the *c*-ring into elastic strain of the γ-subunit. Our observation favors models in which the process of energy transduction from the γ-subunit to the catalytic sites in F_1 is subdivided into smaller steps, each involving smaller amounts of free energy. During ATP hydrolysis at least two substeps (within the 120 deg rotary steps per ATP) of the γ-subunit have been observed with single-molecule spectroscopy (*47*), associated with binding of ATP, catalytic reaction, and release of ADP and phosphate from the catalytic sites. A similar stepwise rotation of the γ-subunit has been detected by a single-molecule FRET approach during ATP synthesis (*13*), providing the first hints for substeps. The present data suggest that each of these rotational substeps involves energy transduction to the catalytic sites.

APPENDIX

(A) Calculation of the Equilibrium Constant K_2 from FCS Data. The equilibrium constant of b_2 dissociation is given by eq 2. From eq 8 we obtain $[b_2] = \alpha[N_T] - [b]$. Substituting this into eq 2 and solving for $[b]$ gives

$$[b] = -{}^1/_2K_1 \pm {}^1/_2\sqrt{K_1{}^2 + 4\alpha K_1[N_T]} \quad \text{(A1)}$$

The mass balance for the *b*-subunit is given by

$$[b]_0 = [b] + 2[b_2] + [bF_1] + 2[b_2F_1] \quad \text{(A2)}$$

With $[b_2]$ from eq 8 and $[b_2F_1]$ from eq 9 we obtain from eq A2

$$[b]_0 = 2[N_T] - [b] - [bF_1] \quad \text{(A3)}$$

The mass balance for F_1 is given by

$$[F_1]_0 = [F_1] + [bF_1] + [b_2F_1] \quad \text{(A4)}$$

With $[b_2F_1] + [bF_1] = (1 - \alpha)[N_T]$ (eq 9) we obtain

$$[F_1]_0 = [F_1] + (1 - \alpha)[N_T] \quad \text{(A5)}$$

The ratio of the equilibrium constants K_4 (eq 4) and K_3 (eq 5) is given by

$$\frac{K_4}{K_3} = \frac{[F_1][b_2F_1]}{[bF_1]^2} \quad \text{(A6)}$$

We substitute into eq A6 $[F_1]$ by eq A5, $[b_2F_1]$ by eq 9, and solve for $[bF_1]$:

$$[bF_1] = \left(2\frac{K_4}{K_3}\right)^{-1}\left[([N_T](1-\alpha) - [F_1]_0) \pm \left([F_1]_0 - (1-\alpha)[N_T])^2 + 4\frac{K_4}{K_3}(1-\alpha)[N_T]([F_1]_0 - [N_T](1-\alpha)\right)\right]^{1/2}\right] \quad \text{(A7)}$$

We substitute eq A7 and eq A1 into eq A3 and we obtain eq A8, which contains the initial concentrations $[b]_0$ and $[F_1]_0$, the fraction of molecules with the short diffusion time, α, the equilibrium constant K_1, the ratio of equilibrium constant K_4/K_3, and the total concentration of fluorescent molecules $[N_T]$:

$$[b]_0 - 2[N_T] + \frac{1}{2}(-K_1 + [K_1{}^2 + 4\alpha K_1[N_T]]^{1/2}) + \left(2\frac{K_4}{K_3}\right)^{-1}\left[([N_T](1-\alpha) - [F_1]_0) \pm \left([F_1]_0 - (1-\alpha)[N_T])^2 + 4\frac{K_4}{K_3}(1-\alpha)[N_T]([F_1]_0 - [N_T](1-\alpha)\right)\right]^{1/2}\right] = 0 \quad \text{(A8)}$$

(B) Calculation of the Equilibrium Constant K_2 from Fluorescence Decrease. We substitute eqs A2 and A4 into eq 6 and we obtain

$$K_p = \frac{([b]_0 - 2[b_2] - [bF_1] - 2[b_2F_1])^2([F_1]_0 - [bF_1] - [b_2F_1])}{[b_2F_1]} \quad \text{(A9)}$$

From eqs 3 and A4 we obtain

$$[b_2] = \frac{K_2[b_2F_1]}{[F_1]_0 - [bF_1] - [b_2F_1]} \quad \text{(A10)}$$

By inserting eq A10 into eq A9 we obtain after rearrangement:

$$K_p = ([b]_0[F_1]_0 - ([b]_0 + 2[F_1]_0 + 2K_2)[b_2F_1] + 3[b_2F_1][bF_1] - ([b]_0 + [F_1]_0)[bF_1] + 2[b_2F_1]^2 + [bF_1]^2)^2/\{[b_2F_1]([F_1]_0 - [b_2F_1] - [bF_1])\} \quad \text{(A11)}$$

The maximal fluorescence decrease is observed when all F_1 contains two bound *b*-subunits:

$$\Delta F_{max} \sim [b_2F_1]_{max} \sim [F_1]_0 \quad \text{(A12)}$$

In the following we discuss two models for fluorescence decrease:

(1) The binding of the first *b*-subunit leads to the same fluorescence decrease as the binding of the second *b*-subunit, which also means that the fluorescence decrease obtained by sequential binding of two *b*-subunits is identical to that by binding of b_2:

$$\Delta F \sim \frac{1}{2}[bF_1] + [b_2F_1] \quad \text{(A13)}$$

From eqs A12 and A13 we obtain

$$\frac{\Delta F}{\Delta F_{max}}[F_1]_0 = \frac{1}{2}[bF_1] + [b_2F_1] = A \quad \text{(A14)}$$

By substituting $[b_2F_1]$ from eq A14 into eq A11, we obtain after rearrangement:

$$K_1K_2\left(A - \frac{[bF_1]}{2}\right)\left([F_1]_0 - A - \frac{[bF_1]}{2}\right) = \left[[b]_0[F_1]_0 - ([b_0] + 2[F_1]_0 + 2K_2)A + 2A^2 + \left(A + K_2 - \frac{[b]_0}{2}\right)[bF_1]\right]^2 \quad \text{(A15)}$$

The unknown parameters in eq A15 are K_1, K_2, and $[bF_1]$.

By combining eq A2 through eq A6, the concentration of $[bF_1]$ can be expressed as a function of A and of the K_4/K_3 ratio as follows:

$$[bF_1] = \frac{[F_1]_0 - \sqrt{[F_1]_0^2 - 4A([F_1]_0 - A)(1 - 4K_4/K_3)}}{1 - 4K_4/K_3} \quad \text{(A16)}$$

In eq A16 the unknown parameter is the ratio K_4/K_3. $[F_1]_0$ and $[b_2]_0$ are known and A is measured.

At the half-maximal fluorescence decrease, when

$$A = \frac{\Delta F}{\Delta F_{max}}[F_1]_0 = \frac{1}{2}[F_1]_0$$

eq A15 simplifies to

$$K_p = K_1K_2 = ([b(^1/_2)]_0 - [F_1]_0 - 2K_2)^2 \quad \text{(A17)}$$

where $[b(^1/_2)]_0$ is the initial b concentration at half-maximal fluorescence decrease, and its value is obtained from the data in Figure 7; i.e., $[b(^1/_2)]_0 = 67$ nM.

From eq A17 we obtain for K_2

$$K_2 = [-(4[F_1]_0 - 4[b(^1/_2)]_0 - K_1) + [(4[F_1]_0 - 4[b(^1/_2)]_0 - K_1)^2 - 16([b(^1/_2)]_0 - [F_1]_0)^2]^{1/2}]/8 \quad \text{(A18)}$$

Therefore, if K_1 is known, K_2 can be obtained from the known $[F_1]_0$ and $[b(^1/_2)]_0$ values. The equilibrium constant K_1 was found to be 1.8 μM, and we obtain from eq A18 $K_2 = 0.6$ nM.

(2) The binding of the first *b*-subunit leads to maximal fluorescence decrease; the binding of the second *b*-subunit does not contribute to fluorescence decrease. This implies that binding of b or b_2 leads to the same fluorescence decrease.

In this case we obtain instead of eq A14 the equation:

$$\frac{\Delta F}{\Delta F_{max}}[F_1]_0 = A = [bF_1] + [b_2F_1] \quad \text{(A19)}$$

By substituting $[bF_1]$ from eq A19 into eq A11 we obtain

$$K_1K_2(A - [bF_1])([F_1]_0 - A) = [[b]_0[F_1]_0 - ([b]_0 + 2[F_1]_0 + 2K_2)A + ([F_1]_0 - A + 2K_2)[bF_1] + 2A^2]^2 \quad \text{(A20)}$$

The unknown parameters in eq A20 are K_1, K_2, and $[bF_1]$.

By combining eq A2 through eq A6, the concentration of $[bF_1]$ can be expressed as a function of A and of the K_4/K_3 ratio as follows:

$$[bF_1] = \left[A - [F_1]_0 + \left[([F_1]_0 - A)^2 + 4\frac{K_4}{K_3}A([F_1]_0 - A)\right]^{1/2}\right]/2\frac{K_4}{K_3} \quad \text{(A21)}$$

When $A = {}^1/_2[F_1]_0$, we obtain K_2 from eqs A20 and A21 as a function of K_1, the ratio K_4/K_3, $[F_1]_0$, and $[b(^1/_2)]_0$, i.e.

$$K_2 = [(4[b(^1/_2)]_0 + K_1 + 4(C - 1)[F_1])_0 + [K_1^2 + 8[b(^1/_2)]_0K_1 + 8(C - 1)[F_1])_0K_1]^{1/2}/8(1 - 2C) \quad \text{(A22)}$$

with

$$C = \frac{-1 + \left[1 + 4\frac{K_4}{K_3}\right]^{1/2}}{4\frac{K_4}{K_3}} \quad \text{(A23)}$$

With $K_1 = 1.8$ μM and $[b(^1/_2)]_0$ from the data in Figure 7, we obtain K_2 from eq A22 as a function of the K_4/K_3 ratio.

REFERENCES

1. Boyer, P. D. (1998) ATP synthase—past and future, *Biochim. Biophys. Acta 1365*, 3−9.
2. Capaldi, R. A., and Aggeler, R. (2002) Mechanism of the F_1F_0-type ATP synthase, a biological rotary motor, *Trends Biochem. Sci. 27*, 154−160.
3. Fillingame, R. H., Angevine, C. M., and Dmitriev, O. Y. (2002) Coupling proton movements to c-ring rotation in F_1F_0 ATP synthase: aqueous access channels and helix rotations at the a−c interface, *Biochim. Biophys. Acta 1555*, 29−36.
4. Weber, J., and Senior, A. E. (2003) ATP synthesis driven by proton transport in F_1F_0-ATP synthase, *FEBS Lett. 545*, 61−70.
5. Boyer, P. D. (1993) The binding change mechanism for ATP synthase—some probabilities and possibilities, *Biochim. Biophys. Acta 1140*, 215−250.
6. Abrahams, J. P., Leslie, A. G. W., Lutter, R., and Walker, J. E. (1994) Structure at 2.8 Å resolution of F_1-ATPase from bovine heart mitochondria, *Nature 370*, 621−628.
7. Gibbons, C., Montgomery, M. G., Leslie, A. G. W., and Walker, J. E. (2000) The structure of the central stalk in bovine F_1-ATPase at 2.4 Å resolution, *Nat. Struct. Biol. 7*, 1055−1061.
8. Engelbrecht, S., and Junge, W. (1997) ATP synthase: an electrochemical transducer with rotatory mechanics, *FEBS Lett. 414*, 485−491.
9. Yoshida, M., Muneyuki, E., and Hisabori, T. (2001) ATP synthase—a marvellousrotary engine of the cell, *Nat. Rev. Mol. Cell. Biol. 2*, 669−677.
10. Kaim, G., Prummer, M., Sick, B., Zumofen, G., Renn, A., Wild, U. P., and Dimroth, P. (2002) Coupled rotation within single F0F1 enzyme complexes during ATP synthesis or hydrolysis, *FEBS Lett. 525*, 156−163.
11. Börsch, M., Diez, M., Zimmermann, B., Reuter, R., and Gräber, P. (2002) Stepwise rotation of the γ-subunit of EF_0F_1-ATP synthase observed by intramolecular single-molecule fluorescence resonance energy transfer, *FEBS Lett. 527*, 147−152.
12. Börsch, M., Diez, M., Zimmermann, B., Trost, M., Steigmiller, S., and Gräber, P. (2003) Stepwise rotation of the γ-subunit of EF_0F_1-ATP synthase during ATP synthesis: a single-molecule FRET approach, *Proc. SPIE—Int. Soc. Opt. Eng. 4962*, 11−21.
13. Diez, M., Zimmermann, B., Börsch, M., König, M., Schweinberger, E., Steigmiller, S., Reuter, R., Felekyan, S., Kudryavtsev, V., Seidel, C. A. M., and Gräber, P. (2004) Proton-powered subunit rotation in single membrane-bound F_0F_1-ATP synthase, *Nat. Struct. Biol.* (in press).
14. Böttcher, B., Schwarz, L., and Gräber P. (1998) Direct indication for the existence of a double stalk in CF_0F_1, *J. Mol. Biol. 281*, 757−762.
15. Wilkens, S., and Capaldi, R. A. (1998) Electron microscopic evidence of two stalks linking the F_1 and F_0 parts of the *Escherichia coli* ATP synthase, *Biochim. Biophys. Acta 1365*, 93−97.
16. Karrasch, S., and Walker, J. E. (1999) Novel features in the structure of bovine ATP synthase, *J. Mol. Biol. 290*, 379−384.
17. Dunn, S. D., McLachlin, D. T., and Revington, M. (2000) The Second Stalk of *Escherichia coli* ATP Synthase, *Biochim. Biophys. Acta 1458*, 356−363.
18. Dimroth, P., Wang, H., Grabe, M., and Oster, G. (1999) Energy transduction in the sodium F-ATPase of Propionigenium modestum, *Proc. Natl. Acad. Sci. U.S.A. 96*, 4924−4929.
19. Häsler, K., Pänke, O., and Junge, W. (1999) On the stator of rotary ATP synthase: the binding strength of subunit δ to $(\alpha\beta)_3$ as determined by fluorescence correlation spectroscopy, *Biochemistry 38*, 13759−13765.

20. Dunn, S. D. (1992) The polar domain of the *b* subunit of *Escherichia coli* F_1F_0-ATPase forms an elongated dimer that interacts with the F_1 sector, *J. Biol. Chem. 267*, 7630−7636.
21. Dunn, S. D., and Chandler, J. (1998) Characterization of a $b_2\delta$ complex from *Escherichia coli* ATP synthase, *J. Biol. Chem. 273*, 8646−8651.
22. Rodgers, A. J., and Capaldi, R. A. (1998) The second stalk composed of the *b*- and δ-subunits connects F_0 to F_1 via an α-subunit in the *Escherichia coli* ATP synthase, *J. Biol. Chem. 273*, 29406−29410.
23. McLachlin, D. T., Coveny, A. M., Clark, S. M., and Dunn, S. D. (2000) Site-directed cross-linking of *b* to the α, β, and *a* subunits of the *Escherichia coli* ATP synthase, *J. Biol. Chem. 275*, 17571−17577.
24. Wilkens, S, Zhou, J, Nakayama, R., Dunn, S. D., and Capaldi, R. A. (2000) Localization of the δ subunit in the *Escherichia coli* F_1F_0-ATPsynthase by immuno electron microscopy: the δ subunit binds on top of the F_1, *J. Mol. Biol. 295*, 387−391.
25. Suzuki, T., Suzuki, J., Mitome, N., Ueno, H., and Yoshida, M. (2000) Second stalk of ATP synthase. Cross-linking of γ-subunit in F_1 to truncated F_0 *b* subunit prevents ATP hydrolysis, *J. Biol. Chem. 275*, 37902−37906.
26. Aggeler, R., and Capaldi, R. A. (1992) Cross-linking of the γ subunit of the *Escherichia coli* ATPase (ECF_1) via cysteines introduced by site-directed mutagenesis, *J. Biol. Chem. 267*, 21355−21359.
27. Gogol, E. P., Aggeler, R., Sagermann, M., and Capaldi, R. A. (1989) Cryoelectron microscopy of *Escherichia coli* F_1 adenosinetriphosphatase decorated with monoclonal antibodies to individual subunits of the complex, *Biochemistry 28*, 4717−4724.
28. Turina, P., and Capaldi, R. A. (1994) ATP hydrolysis-driven structural changes in the γ-subunit of *Escherichia coli* ATPase monitored by fluorescence from probes bound at introduced cysteine residues, *J. Biol. Chem. 269*, 13465−13471.
29. Gill, S. C., and von Hippel, P. H. (1989) Calculation of protein extinction coefficients from amino acid sequence data, *Anal. Biochem. 182*, 319−326.
30. McLachlin, D. T., and Dunn, S. D. (1997) Dimerization interactions of the *b* subunit of the *Escherichia coli* F_1F_0-ATPase, *J. Biol. Chem. 272*, 21233−21239.
31. Aitken, A., and Learmonth, M. P. (2003) in *The Protein Protocols Handbook* (Walker, J. M., Ed.) 2nd ed., pp 3−6, Humana Press, Totowa, NJ.
32. Zamyatin, A. A. (1984) Amino acid, peptide, and protein volume in solution, *Annu. Rev. Biophys. Bioeng. 13*, 145−165.
33. Widengren, J., Mets, Ü., and Rigler, R. (1995) Fluorescence correlation spectroscopy of triplet states in solution: a theoretical and experimental study, *J. Phys. Chem. 99*, 13368−13379.
34. Revington, M., McLachlin, D. T., Shaw, G. S., and Dunn, S. D. (1999) The dimerization domain of the *b* subunit of the *Escherichia coli* F_1F_0-ATPase, *J. Biol. Chem. 274*, 31094−31101.
35. Revington, M., Dunn, S. D., and Shaw, G. S. (2002) Folding and stability of the *b* subunit of the F_1F_0 ATP synthase, *Protein Sci. 11*, 1227−1238.
36. Del Rizzo, P. A., Bi, Y., Dunn, S. D., and Shilton, B. H. (2002) The "second stalk" of *Escherichia coli* ATP synthase: structure of the isolated dimerization domain, *Biochemistry 41*, 6875−6884.
37. Börsch, M., Turina, P., Eggeling, C., Fries, J. R., Seidel C. A. M., Labahn A., and Gräber, P. (1998) Conformational changes of the H^+-ATPase from *Escherichia coli* upon nucleotide binding detected by single molecule fluorescence, *FEBS Lett. 437*, 251−254.
38. Mendel-Hartvig, J., and Capaldi, R. A. (1991) Structure−function relationships of domains of the δ subunit in *E. coli* adenosine triphosphatase, *Biochim. Biophys. Acta 1060*, 115−124.
39. Ziegler, M., Xiao, R., and Penefsky, H. S. (1994) Close proximity of Cys64 and Cys140 in the δ subunit of *Escherichia coli* F_1-ATPase, *J. Biol. Chem. 269*, 4233−4239.
40. McLachlin, D. T., Bestard, J. A., and Dunn, S. D. (1998) The *b* and δ subunits of the *Escherichia coli* ATP synthase interact via residues in their C-terminal regions, *J. Biol. Chem. 273*, 15162−15168.
41. Duncan, T. M., Bulygin, V. V., Zhou, Y., Hutcheon, M. L., and Cross, R. L. (1995) Rotation of subunits during catalysis by *Escherichia coli* F_1-ATPase, *Proc. Natl. Acad. Sci. U.S.A. 92*, 10964−10968.
42. Sabbert, D., Engelbrecht, S., and Junge, W. (1996) Intersubunit rotation in active F-ATPase, *Nature 381*, 623−625.
43. Noji, H., Yasuda, R., Yoshida, M., and Kinosita, K., Jr. (1997) Direct observation of the rotation of F_1-ATPase, *Nature 386*, 299−302.
44. Pänke, O, and Rumberg, B. (1999) Kinetic modeling of rotary CF_0F_1-ATP synthase: storage of elastic energy during energy transduction, *Biochim. Biophys. Acta 1412*, 118−128.
45. Oster, G., and Wang, H. (2000) Reverse engineering a protein: the mechanochemistry of ATP synthase, *Biochim. Biophys. Acta 1458*, 482−510.
46. Cross, R. L. (2000) The rotary binding change mechanism of ATP synthases, *Biochim. Biophys. Acta 1458*, 270−275.
47. Yasuda, R., Noji, H., Yoshida, M., Kinosita, K., Jr., and Itoh, H. (2001) Resolution of distinct rotational sub-steps by submillisecond kinetic analysis of F_1-ATPase, *Nature 410*, 898−904.

BI0357098